JACS
JOURNAL OF THE AMERICAN CHEMICAL SOCIETY
Article
pubs.acs.org/JACS

Evidence for Halogen Bond Covalency in Acyclic and Interlocked Halogen-Bonding Receptor Anion Recognition

Sean W. Robinson,[†] Chantal L. Mustoe,[‡] Nicholas G. White,[†,‡] Asha Brown,[†] Amber L. Thompson,[†] Pierre Kennepohl,*[,‡] and Paul D. Beer*[,†]

[†]Chemistry Research Laboratory, Department of Chemistry, University of Oxford, Mansfield Road, Oxford OX1 3TA, U.K.
[‡]Department of Chemistry, University of British Columbia, 2036 Main Mall, Vancouver, British Columbia, Canada V6T 1Z1

Supporting Information

ABSTRACT: The synthesis and anion binding properties of novel halogen-bonding (XB) bis-iodotriazole-pyridinium-containing acyclic and [2]catenane anion host systems are described. The XB acyclic receptor displays selectivity for acetate over halides with enhanced anion recognition properties compared to the analogous hydrogen-bonding (HB) acyclic receptor. A reversal in halide selectivity is observed in the XB [2]catenane, in comparison to the acyclic XB receptor, due to the interlocked host's unique three-dimensional binding cavity, and no binding is observed for oxoanions. Notable halide anion association constant values determined for the [2]catenane in competitive organic−aqueous solvent mixtures demonstrate considerable enhancement of anion recognition as compared to the HB catenane analogue. X-ray crystallographic analysis of a series of halide catenane complexes reveal strong XB interactions in the solid state. These interactions were studied using Cl and Br K-edge X-ray Absorption Spectroscopy (XAS) indicating intense pre-edge features characteristic of charge transfer from the halide to its bonding partner ($\sigma^*_{AX\leftarrow X^-} \leftarrow X1s$), and providing a direct measure of the degree of covalency in the halogen bond(s). The data reveal that the degree of covalency is similar to that which is observed in transition metal coordinate covalent bonds. These results are supported by DFT results, which correlate well with the experimental data.

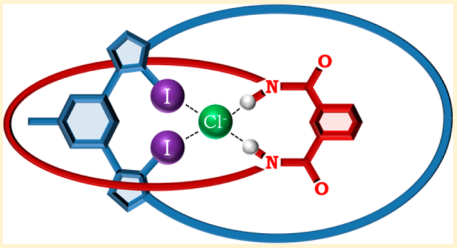

INTRODUCTION

Halogen bonding (XB) refers to the attractive noncovalent interaction arising between the electron-deficient σ-hole of a polarized halogen atom, such as bromine or iodine, and an electron-rich Lewis base.[1−4] While XB has been well-developed in the context of solid-state crystal engineering[5−12] and in the design of functional materials,[9,13−15] the utilization of XB in solution is relatively underexploited with seminal applications in the areas of reactivity,[16−18] catalysis,[19,20] self-assembly,[21,22] transport,[23] and medicinal chemistry only recently being reported.[24] Anion supramolecular chemistry has experienced rapid growth over the past few decades stimulated by the crucial roles that anions play in many chemical, biological, and environmental processes.[25−37] While supramolecular interactions such as hydrogen bonding (HB) have dominated the field of anion coordination, recognition, and transport,[38−51] halogen bonding (XB) has only recently begun to emerge as a powerful alternative interaction capable of coordinating anions in competitive solvent media.[21,52−60] The strength of XB in solution has been demonstrated to be comparable to HB,[9] while the stringent linear directionality of XB and pH-independence is advantageous for the design of selective receptors for anions with particular geometries. It is noteworthy that the relatively few examples of acyclic and macrocyclic XB anion receptors reported to date all display significantly contrasting anion recognition behavior compared to HB analogues. Furthermore, rotaxane interlocked host structural frameworks containing convergent XB triazolium donor groups have been demonstrated to selectively recognize and sense halide anions in highly competitive aqueous media.[59,61,62]

Herein we report a bis-iodotriazole-pyridinium motif, incorporated within both an acyclic and a novel catenane-based receptor, capable of binding anions via two convergent R−I···X$^-$ halogen bonds. The [2]catenane host structural framework, prepared via chloride anion templation, is demonstrated to bind halide anions with impressive selectivity in competitive organic−aqueous solvent mixtures.

In addition, we report for the first time Cl and Br K-edge XAS analysis of the interactions observed in these receptors with anions, revealing significant charge transfer from the halides to the iodotriazole XB donors, and the first measure of covalency in these systems. These data allow for the first quantitative evaluation of the degree of covalency in halogen-bonded species. Pre-edge features in the XAS spectra are modeled and supplemented with DFT calculations and TDDFT simulations of the XAS data which reproduce the experimentally observed pre-edge features.

RESULTS AND DISCUSSION

Acyclic Receptors. *Synthesis.* The synthesis of the acyclic bis-triazole-pyridinium receptors is shown in Scheme 1. 3,5-

Received: November 12, 2014
Published: December 5, 2014

   dx.doi.org/10.1021/ja511648d | J. Am. Chem. Soc. 2015, 137, 499−507

Scheme 1. Synthesis of Acyclic Receptors 3a–d·A[a]

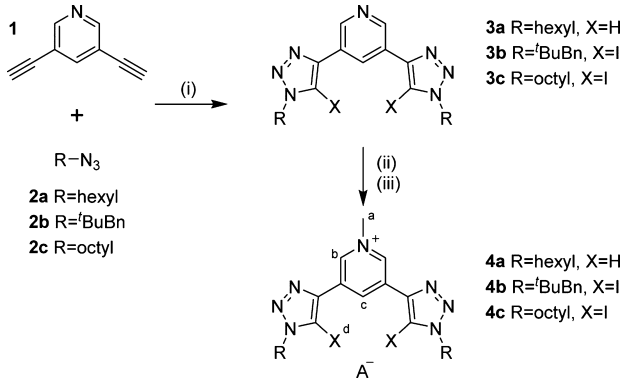

[a]Reagents and conditions: (i) X = H: $CuSO_4·5H_2O$, ascorbic acid, Na_2CO_3, NaN_3, hexyl-bromide, **3a**: 79%;[66] X = I: NaI, $Cu(ClO_4)_2·6H_2O$, TBTA, DBU, THF, **3b**: 76%, **3c**: 79%; (ii) CH_3I, DCM, **4a**·I: 81%, **4c**·I: 80%; (iii) $NH_4PF_{6(aq)}$, **4a**·PF_6: 89%, **4b**·PF_6: 53%.

Diethynylpyridine **1** was prepared by deprotecting 3,5-bis-(trimethylsilylethynyl) pyridine[63] with KOH in methanol,[64] while azides **2a–c**[65] were prepared via a modification of a literature procedure. The bidentate bis-triazole-pyridinium acyclic precursor, **3a**, was prepared via a CuAAC "click" reaction between **1** and 2.2 equiv of hexylazide, prepared *in situ* from the corresponding bromide.[66] The bidentate bis-iodotriazole-pyridinium acyclic receptor precursors, **3b** and **3c**, were prepared using a modification of a CuAAC "click" reaction literature procedure using various azides.[67] Subsequent methylation with CH_3I afforded acyclic receptors **4a–c**·I which were characterized by high-resolution ESI mass spectrometry, ^1H, ^{13}C NMR, and ^{19}F as well as ^{31}P NMR spectroscopy where appropriate. Acyclic receptors **4a** and, for solubility reasons, **4b** were anion exchanged to their corresponding noncoordinating hexafluorophosphate salts in preparation for anion titration experiments, while **4c**·X was used in X-ray crystallographic structure analysis (X = Cl^-) and X-ray absorption spectroscopic analysis (X = Cl^-, Br^-, PF_6^-).

^1H NMR Anion Recognition Studies. The anion recognition properties of acyclic receptors **4a**·PF_6 and **4b**·PF_6 were investigated using ^1H NMR anion titration experiments by adding aliquots of anions as their tetrabutylammonium salts to solutions of the receptor. Initial titrations with TBA·Cl in acetone-d_6 determined 1:1 stoichiometric association constants of $>10^4$ M^{-1} for both receptors. Consequently, titrations were repeated in the more competitive CD_3CN affording the data in Table 1 for HB receptor **4a**·PF_6; however, association constants for XB receptor **4b**·PF_6 were still $>10^4$ M^{-1}. As a result, titrations for **4b**·PF_6 were performed in the even more competitive solvent DMSO-d_6 indicating the superior anion-binding capability of the XB receptor. Addition of anions typically caused downfield perturbations of **4a**·PF_6 triazole proton *d*, directly involved in anion coordination, and the **4b**·PF_6 pyridinium proton *c* incumbent on anion binding (Figure 1). WinEQNMR2[68] analysis of the titration data determined the 1:1 stoichiometric association constants shown in Table 1.

The anion binding selectivity of prototriazole receptor **4a**·PF_6 follows anion basicity trends, as would be expected for an anion receptor in an aprotic solvent, with the larger halides complexed more weakly than chloride.

Similarly, for the XB acyclic receptor **4b**·PF_6, selectivity follows anion basicity trends for the halides, with OAc^- being the most strongly associated anion; the association constant, K_a, is 2.5 times larger in magnitude than chloride. Interestingly, no binding was observed for $H_2PO_4^-$ and NO_3^-, while SO_4^{2-} was bound at $>10^4$ M^{-1}, presumably due to the greater negative charge. To the best of our knowledge, this is only the second example of an XB oxoanion-selective anion receptor.[60]

Table 1. Association Constants, K_a (M^{-1})[a] for 4a·PF_6 and 4b·PF_6

	K_a (M^{-1})	
anion	**4a**·PF_6 (CD_3CN)[66]	**4b**·PF_6 (DMSO-d_6)
Cl^-	206(11)	387(20)
Br^-	106(3)	238(12)
I^-	59(2)	146(3)
OAc^-	–[b]	1025(9)
$H_2PO_4^-$	precipitation	NB[c]
NO_3^-	–[b]	NB[c]
SO_4^{2-}	–[b]	$>10^4$

[a]Calculated using WinEQNMR2[68] monitoring the chemical shift data of **4a**·PF_6 proton *d* and **4b**·PF_6 proton *c*; estimated standard errors given in parentheses (298 K). [b]Not conducted. [c]NB: No binding: $\Delta\delta$ < 0.04 ppm.

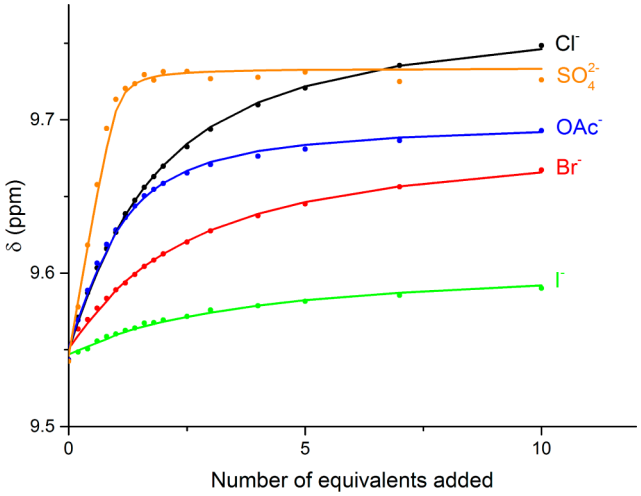

Figure 1. Anion binding titrations with **4b**·PF_6 following proton *c* in DMSO-d_6: experimental titration data (circles) with fitted binding isotherms indicated as lines (298 K).

X-ray Crystallography.[69] Crystals suitable for X-ray diffraction structural analysis were obtained from the chloride salt of the octyl-appended acyclic receptor **4c**·Cl. The solid-state structure displays convergent iodotriazole–I···Cl^- halogen bonds (Figure 2) and planarity across the iodotriazole–pyridinium–iodotriazole heterocyclic motif, despite the large size of the iodine substituents (Figure 2). The asymmetric unit consists solely of one molecule of **4c**·Cl. The chelating XBs vary in length from 3.121(2) to 3.195(2) Å corresponding to 84–86% of the sum of the van der Waals halide radii, which is indicative of strong XB interactions to the anion.[70]

[2]Catenane. *Synthesis of XB Catenane 9·PF_6.* As a result of the enhanced anion recognition properties of the acyclic XB receptor **4b**·PF_6, in comparison to the HB analogue, **4a**·PF_6, the bis-iodotriazole-pyridinium motif was integrated into a [2]-catenane host structural framework. To this end, macrocycle precursor **6** was prepared initially, by reaction of **1** with 2.2 equiv of vinyl-appended azide **5**,[64] via the same modified CuAAC methodology (Scheme 2). Methylation was achieved

dx.doi.org/10.1021/ja511648d | J. Am. Chem. Soc. 2015, 137, 499–507

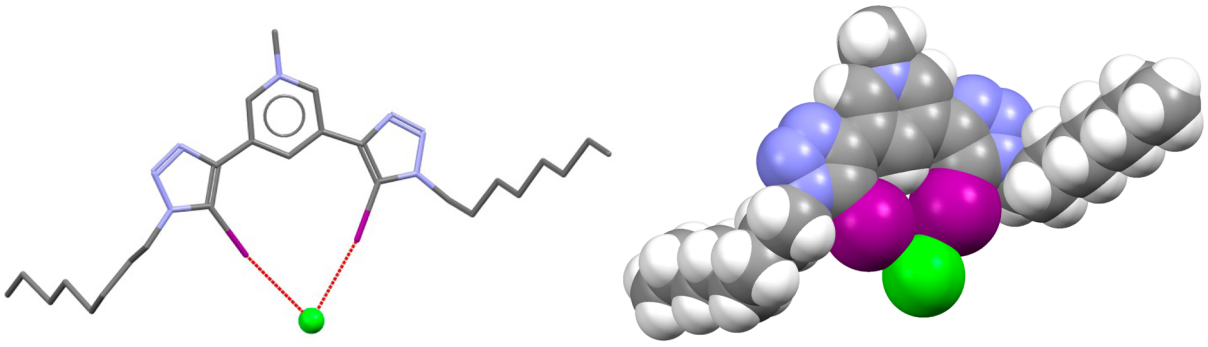

Figure 2. Perspective (left) and space-filling representation (right) views of the crystal structure of **4c**·Cl. Triazole–I···Cl^- halogen bonds (3.121(2)–3.195(2) Å) are indicated as red dashed lines. Hydrogen atoms omitted for clarity. Gray = carbon, blue = nitrogen, purple = iodine, green = chlorine.

Scheme 2. Synthesis of Vinyl-Appended Macrocycle Precursor 7·Cl[a]

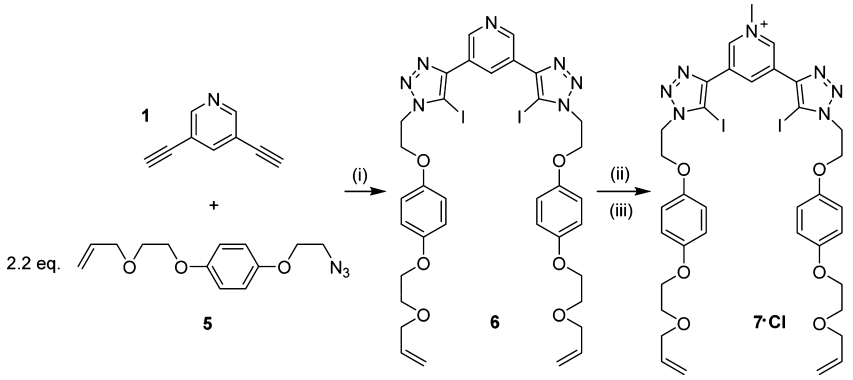

[a]Reagents and conditions: (i) NaI, $Cu(ClO_4)_2·6H_2O$, TBTA, DBU, THF, 56%; (ii) CH_3I, DCM, 99%; (iii) $NH_4Cl_{(aq)}$, 66%.

using CH_3I, and thereafter, the vinyl-appended bis-iodotriazole-pyridinium-containing macrocycle precursor was anion exchanged to the corresponding chloride salt by repeated washing with $NH_4Cl_{(aq)}$ to afford **7**·Cl.

Synthesis of [2]catenane **9**·Cl was accomplished using chloride templation via a ring-closing metathesis strategy. An initial interpenetrated assembly was prepared by mixing equimolar amounts of macrocycle **8**[71] with **7**·Cl in dry CH_2Cl_2. Addition of Grubbs' II ring-closing metathesis catalyst afforded the [2]catenane in 41% yield following purification by preparative thin layer chromatography.

Catenane **9**·Cl was characterized by ^1H, ^{13}C and 2D COSY NMR experiments and high-resolution mass spectrometry. Notable shifts in the pyridinium and isophthalamide protons *c* and 3, respectively, were observed in addition to the splitting and upfield perturbation of the hydroquinone protons 5 and 6 consistent with inter-ring donor–acceptor interactions between the electron-rich hydroquinone groups and the electron-deficient pyridinium group, which confirms the interlocked nature of the catenane (Figure 3). Further evidence for the interlocking of the two macrocyclic components was obtained by 2D ROESY NMR which revealed through-space interactions including those between hydroquinone and pyridinium protons of the two macrocycles (see Supporting Information (SI)).

The chloride anion template was removed by repeated washing with $NH_4PF_{6(aq)}$ to afford **9**·PF_6 for anion recognition studies and was similarly fully characterized (Scheme 3).

^1H NMR Anion Recognition Studies. Association constants for the formation of 1:1 stoichiometric host/guest complexes of catenane **9**·PF_6 with various anions were determined using ^1H

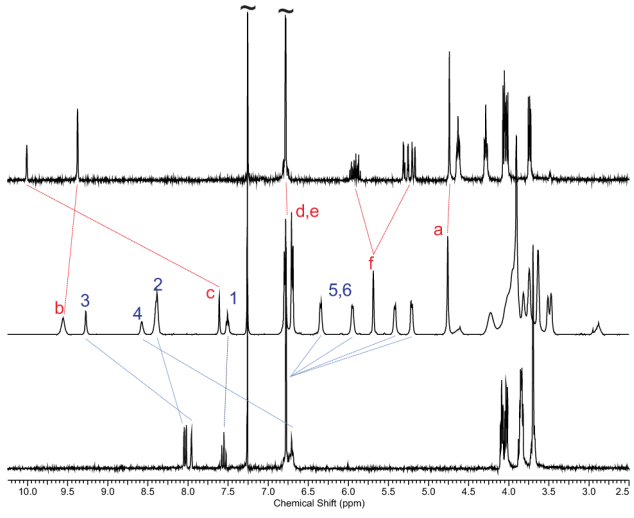

Figure 3. Truncated ^1H NMR spectra of **7**·Cl (top), **9**·Cl (middle), and **8** (bottom) (300 MHz, 293 K, solvent: $CDCl_3$).

NMR titration experiments, monitoring shifts in the internal isophthalamide proton 3 upon addition of aliquots of anions added as their tetrabutylammonium salts (Figure 4).[72] A preliminary titration of **9**·PF_6 with TBA·Cl in 1:1 $CDCl_3$/CD_3OD resulted in an association constant $K_a > 10^4$ M^{-1}, much greater than the value obtained for the previously reported analogous prototriazole-containing HB catenane (Table 2).[64] Consequently, all subsequent titrations were conducted in the aqueous solvent mixture 10:45:45 D_2O/

dx.doi.org/10.1021/ja511648d | J. Am. Chem. Soc. 2015, 137, 499–507

Scheme 3. Synthesis of [2]Catenane 9·PF$_6$[a]

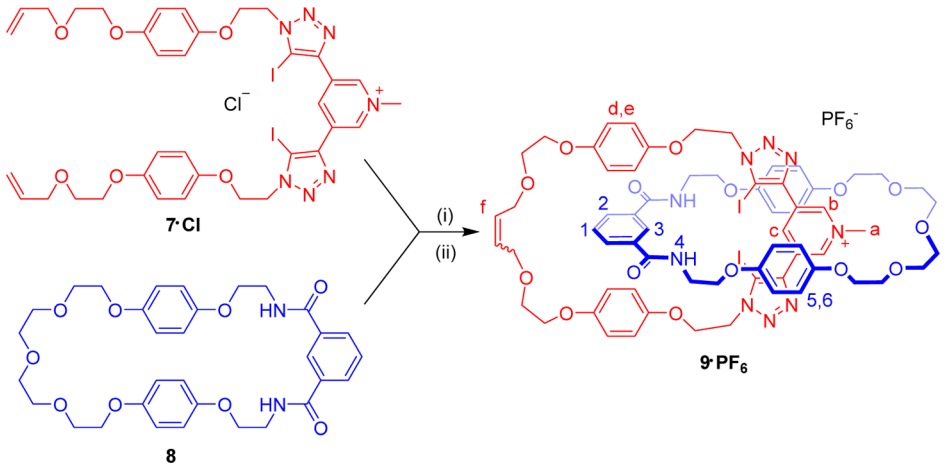

[a]Reagents and conditions: (i) Grubbs' II (10 wt %), DCM, 41%; (ii) $NH_4PF_{6(aq)}$, 86%.

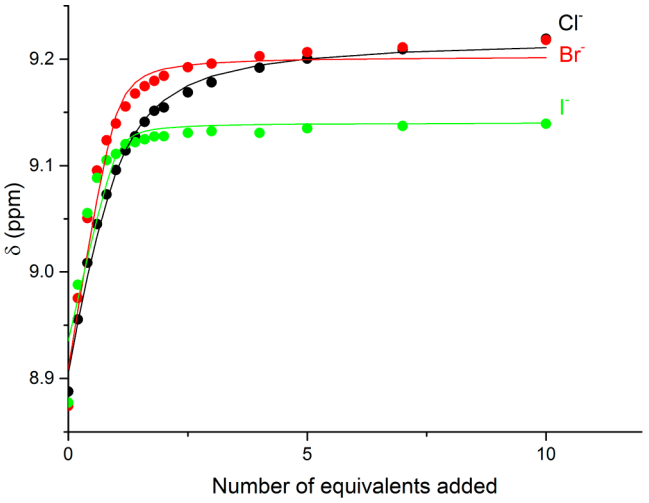

Figure 4. Anion binding titrations with 9·PF$_6$ following isophthalamide proton 3 in 10:45:45 $D_2O/CDCl_3/CD_3OD$: experimental titration data (circles) with calculated fit indicated as the line (298 K).

Table 2. Association Constants, K_a (m^{-1})[a] for 9·PF$_6$

	K_a (m^{-1})	
anion	HB catenane[64,b]	9·PF$_6$
Cl^-	680(20)	1850(224)
Br^-	630(50)	$>10^4$
I^-	510(10)	$>10^4$
OAc^-	–[c]	NB[d]
$H_2PO_4^-$	49(4)	NB[d]

[a]Calculated using WinEQNMR2[68] monitoring the internal pyridinium proton; estimated standard errors given in parentheses (293 K, solvent: 10:45:45 $D_2O/CDCl/CD_3OD$). [b]1:1 $CDCl_3/CD_3OD$, 298 K. [c]Not conducted. [d]NB: No binding: $\Delta\delta < 0.07$ ppm.

$CDCl_3/CD_3OD$, which is more competitive. The association constants shown in Table 2 were determined by WinEQNMR2[68] analysis of the titration data.

Very strong binding of the halides is observed for 9·PF$_6$ in this aqueous solvent mixture. Indeed, association constants determined for Br^- and I^- are both $>10^4$ m^{-1} which highlights the fact that binding is dramatically enhanced in the XB catenane when compared to the HB catenane analogue.[73] Furthermore, in contrast, the XB host demonstrates a preference for the larger halides despite the voluminous iodine XB donors. Indeed, a reversal in selectivity for the halides is observed for 9·PF$_6$ in comparison to the acyclic receptor **4b**·PF$_6$ due the interlocked host's unique three-dimensional binding cavity.

Despite the OAc^- selectivity observed for the acyclic XB receptor **4b**·PF$_6$, no evidence for oxoanion binding was discerned for OAc^- or $H_2PO_4^-$ for the XB catenane 9·PF$_6$. This may be attributed to the oxoanions' large size and unfavorable geometry to bind and be encapsulated by the unique interlocked catenane host cavity (*vide infra*).

X-ray Crystallography. Crystals suitable for X-ray diffraction structural analysis were obtained for catenane 9^+ with chloride, bromide, iodide, dihydrogen phosphate, and sulfate counteranions. All structures crystallize in $P\bar{1}$ with 1:1 complexes obtained for chloride (Figure 5), bromide, and iodide, which are isomorphous, and 2:1 complexes were obtained for dihydrogen phosphate and sulfate, which in turn are isomorphous. While both hydrogen and halogen bonds are observed between the host 9^+ and the anionic guest, the catenane curiously adopts an "open" conformation in the solid state rather than completely encapsulating the anion; presumably this is due to the large iodo-substituted triazole and the most energetically favorable conformation for crystallization. While a varying degree of disorder for the polyether ends of the macrocycles is observed in each complex, it does not affect the anion-binding cavity of the catenane and is omitted for clarity here.

Examining the halide anion structures, strong halogen bonds are observed indicated by bond lengths significantly shorter than the sum of the van der Waals radii and are summarized in Table 3.[70]

The structure of $(9)_2·SO_4$ (Figure 6) clearly shows the SO_4^{2-} anion situated between two hosts rather than being encapsulated in the cavity, as it is too large to penetrate the interlocked binding pocket. Furthermore, the anion is on the inversion center in the asymmetric unit allowing it to adopt one of two symmetry-related orientations (see Supporting Information). Two independent S–O···I–C halogen bonds are formed rather than bifurcated halogen bonds from one O to each of the iodine XB donors. The dihydrogen phosphate structure (see Supporting Information), while of lower quality,

dx.doi.org/10.1021/ja511648d | J. Am. Chem. Soc. 2015, 137, 499–507

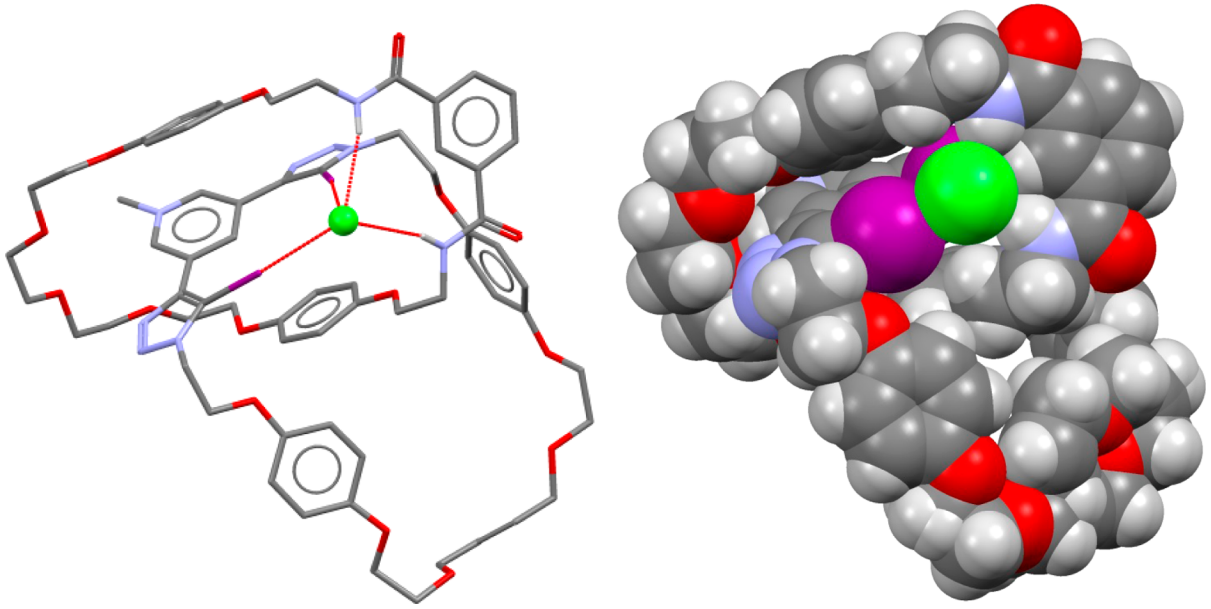

Figure 5. Perspective (left) and space-filling representation (right) views of the crystal structure of **9**·Cl. Triazole–I···Cl^- halogen bonds (3.110(2)–3.300(3) Å) are indicated as red dashed lines. Hydrogen atoms (except amide) omitted for clarity. Gray = carbon, blue = nitrogen, red = oxygen, purple = iodine, green = chlorine, white = hydrogen. For further information regarding the isomorphous **9**·Br and **9**·I structures, see SI.

Table 3. Crystallographically Determined XB Bond Lengths and Percentage Shortening of the Sum of the van der Waals Radii (%VdW)[70]

anion	interatomic distances (I···X^-)[a]	%VdW
Cl^-	3.110(2)–3.305(3)	83–88%
Br^-	3.178(2)–3.359(2)	83–88%
I^-	3.324(1)–3.543(1)	84–89%

[a]Calculated errors given in parentheses.

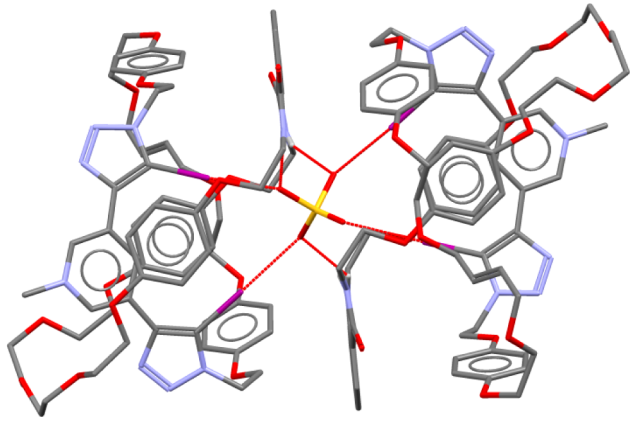

Figure 6. Crystal structure of $(\mathbf{9})_2 \cdot SO_4^{2-}$ showing a 2:1 catenane/anion complex with the anion (SO_4^{2-}) positioned between the two catenane hosts rather than penetrating the binding cavity. XB and HB interactions are shown as red dashed lines. Hydrogen atoms (except amide) omitted for clarity. Gray = carbon, blue = nitrogen, red = oxygen, purple = iodine, white = hydrogen, orange = phosphorus, yellow = sulfur.

shows a very similar structure; i.e., the large oxoanion binds outside of the cavity.

Donor K-edge X-ray Absorption Spectroscopy. To establish the nature of the interactions between the halide (Cl^-/Br^-) donor and the iodine acceptor, we have exploited Cl and Br K-edge X-ray Absorption Spectroscopy (XAS). It has been clearly established that Cl K-edge XAS can be used to evaluate the degree of delocalization in chloro-metal bonds.[74−76] In such cases, a pre-edge feature is observed in the spectrum that formally corresponds to excitation of a Cl_{1s} electron to empty valence *d*-orbitals on the transition metal acceptor. The intensity of such transitions is directly proportional to the amount of Cl_{3p} character mixed into these empty metal acceptor orbitals, providing a convenient method of obtaining a quantitative measure of the degree of mixing between the chloro donor and the metal acceptor. This methodology is equally applicable in cases where nonmetal acceptors are under investigation, although to our knowledge it has not been applied to other types of donor–acceptor systems.

Within the context of this work, one would expect a halide ion (Cl^- and/or Br^-) to exhibit simple K-edge XANES spectra with no pre-edge features. Electric-dipole allowed $Cl_{3p} \leftarrow Cl_{1s}$ (or $Br_{4p} \leftarrow Br_{1s}$) transitions would not be observed since these valence *p*-states are filled (ns^2np^6). Covalent delocalization of the filled Cl_{3p} orbital with an empty acceptor orbital (e.g., via hydrogen or halogen bonding) would result in the possibility of a new allowed transition corresponding to charge transfer from the chloride to its bonding partner ($\sigma^*_{AX\leftarrow Cl} \leftarrow Cl_{1S}$). Given that the intensity of such transitions is directly proportional to the amount of Cl_{3p} in the final state wave function, $\sigma^*_{AX\leftarrow Cl^-}$, the intensity of any observable pre-edge feature provides us a direct measure of the degree of covalency in the halogen bond.

Chlorine K-edge XAS data were obtained for a series of donor–acceptor complexes at beamline 4-3 at the Stanford Synchrotron Radiation Lightsource. The near-edge spectra for **4**·Cl and **9**·Cl (see Figure 7) each exhibit an intense pre-edge feature that is not present in ionic chloride salts. The presence of this intense feature can only result from charge transfer between the chloro donor and its partners.[74,76] Fitting of the pre-edge and edge features allows experimental quantification of the degree of charge donation in each of these species (Table 4).[77−79] These results clearly demonstrate charge transfer from the donor via halogen bonding in **4**·Cl, and a combination of

dx.doi.org/10.1021/ja511648d | J. Am. Chem. Soc. 2015, 137, 499–507

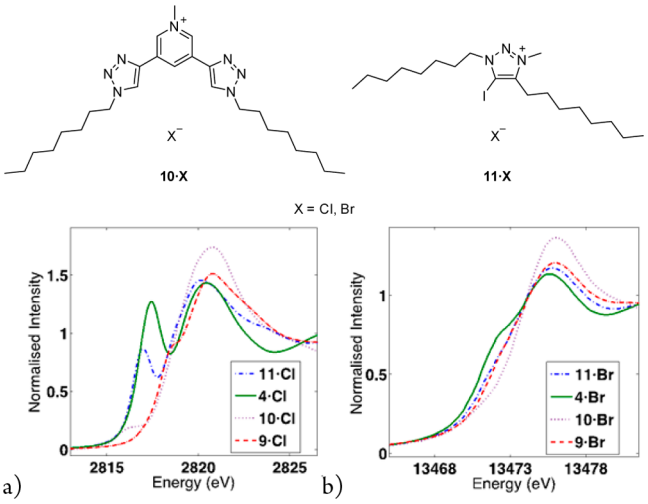

Figure 7. Normalized and background subtracted: (a) Cl K- and (b) Br K-edge XAS data for **11**·Cl/Br, **4**·Cl/Br, **10**·Cl/Br, and **9**·Cl/Br.

Table 4. Experimentally Obtained Pre-edge Intensities and the Corresponding % Charge Donation of Chloride Donor Complexes

	interactions				
compd	$Cl^-\cdots X$	$Cl^-\cdots H$	pre-edge energy (eV)	normalized pre-edge intensity[a]	total donation (% Cl_{3p})[b]
11·Cl	1	–	2816.9(1)	0.90(5)	6.4(2.1)
4·Cl	2	–	2817.3(1)	1.59(4)	11.3(2.0)
10·Cl	–	2	2816.2(2)	0.13(3)	0.9(1.9)
9·Cl	2	2	2818.4(2)	1.00(6)	7.1(2.3)

[a]Calculated errors (parentheses) are obtained from statistical distribution of fit results for >50 fits for each data set. See section S1 for further details. [b]Total donation is calculated in comparison with Cl K-edge XAS data on a $CuCl_4^{2-}$ reference, errors include an estimate of the error in charge transfer of this reference compound.

XB and HB interactions in **9**·Cl. For comparison, data were also collected on the H-bonding analogue of **4**·Cl (**10**·Cl) as well as a simple X-bonded adduct 5-iodo-3-methyl-1,4-dioctyl-1*H*-1,2,3-triazol-3-ium chloride (**11**·Cl) (Figure 7; see SI for the synthesis of **10**·Cl and **11**·Cl). These data provide a measure of the total donation from the chloride anion to all of its bonding partners, and thus the number of interactions must be considered when interpreting these results.

It is apparent that, with a chloride donor, X-bonding interactions are significantly more covalent in character than comparable H-bonding interactions. These data are consistent with previous reports that charge transfer is an important factor in XB bonds.[80] These XAS data, however, allow us to quantify the degree of covalency in the XB bond and thus compare the degree of charge transfer in different systems, which to our knowledge is unprecedented. In **11**·Cl, where only a single halogen bonding interaction is possible, we find that the degree of donation is consistent with ~6% charge transfer to the iodinated triazole acceptor. The magnitude of charge donation/covalent character in the XB bond is notable in that it is a similar magnitude to that which is commonly observed in transition metal complexes, where covalent contributions are considered to be of great importance in defining chemical properties. For example, in simple divalent metal chlorides ($[MCl_4^{2-}]$, where M = Cu, Ni, Co, Fe), bond covalencies have been determined to range from 6% to 9%.[74]

In the bis-triazole **4**·Cl, the total charge donation from the halide ion almost doubles to ~11%, which implies that each of the halogen bonds are independent from each other and additive. By contrast, replacement of the iodine acceptors for protons in the bis-triazole (**10**·Cl) leads to an almost complete loss of intensity in the Cl K-edge XAS pre-edge feature, reflecting very poor charge donation through H-bonding in this system.

Data for the catenane **9**·Cl, where both H- and X-bonds are present, indicate that charge donation from the chloride anion decreases substantially (as compared to **4**·Cl). This presumably reflects weakened halogen bonding due to competition with amide H-bond interactions.

Qualitatively similar data were obtained for the bromide donor complexes **11**·Br, **4**·Br, **10**·Br, and **9**·Br (see Figure 7). Unfortunately, lifetime broadening at the higher energy Br K-edge, as well as smaller energy separation between features, leads to poorer resolution of the pre-edge features of interest. The data indicate the presence of a low-energy shoulder, indicating a pre-edge feature to that observed in the Cl K-edge data. We note that the pre-edge shoulder is larger for the X-bonded systems as compared to the H-bonded system (**10**·Br). However, quantitative comparisons between the different X-bonded systems are inconclusive due to large errors in the associated fits (see section S6).

Computational. To further explore the details of the covalent nature of X-bonding in these systems, we performed a series of density functional calculations, and TDDFT simulations of the XAS data.[81] Optimized geometries (Table 5) are in good agreement with experimental data. For example,

Table 5. DFT-Calculated Parameters Obtained for Halide Adducts[a]

	average bond			
distances (Å)	$X^-\cdots I$	$X^-\cdots H$	total % Cl_{3p} in $\sigma^*_{AX\leftarrow X^-}$	$10^3 * f_{osc}$ for $\sigma^*_{AX\leftarrow X^-} \leftarrow X_{1s}$
11·Cl	3.00	–	6.9	1.292
4·Cl	3.18	–	7.7	1.862
10·Cl	–	2.54	1.1	0.215
9·Cl	3.21	2.62	6.1	–
11·Br	3.21	–	6.4	0.198
4·Br	3.40	–	8.0	0.286
10·Br	–	2.76	1.7	0.045
9·Br	3.41	2.82	5.6	–

[a]All calculated values are for fully optimized structures at the B3LYP/def2-TZVP+ZORA level of theory.

the r_{Cl-I} in **4**·Cl are calculated to be 3.18(3) Å, which compare favorably with that observed crystallographically (3.120(2)–3.195(2) Å). TDDFT simulations of the Cl K- and Br K-edge XAS data reproduce the low energy pre-edge feature assigned to the $\sigma^*_{AX\leftarrow X^-} \leftarrow X_{1s}$ transition in each case. The relevant $\sigma^*_{AX\leftarrow X^-}$ orbitals for **11**·Cl and **4**·Cl are shown in Figure 8. In each case, these antibonding acceptor orbitals reflect the covalent nature of the $X^- \rightarrow I$ bond(s). Two relevant acceptor orbitals are present in **4**·Cl since two $X^- \rightarrow I$ interactions are possible; the splitting of these two orbitals in **4**·Cl is small (~0.3 eV), and thus the resulting transitions cannot be resolved experimentally.

dx.doi.org/10.1021/ja511648d | J. Am. Chem. Soc. 2015, 137, 499–507

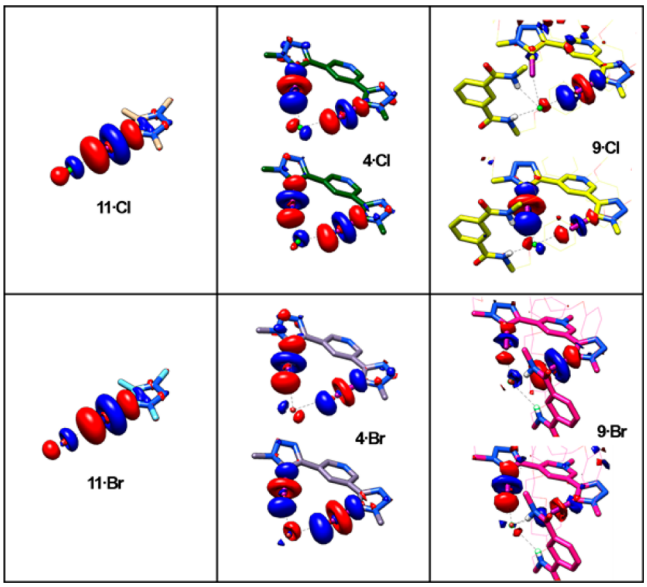

Figure 8. Visual representation of the important $\sigma^*_{AX\leftarrow X^-}$ Kohn−Sham acceptor orbitals for **11**, **4**, and **9**. Surface volumes for each orbital are plotted for ±0.05 $e/Å^3$.

TDDFT-based simulations of the Cl K- and Br K-edge XAS data are in good qualitative agreement with the experimental data (Figure 9). As anticipated, the intensities of the $\sigma^*_{AX\leftarrow X^-}$ ←

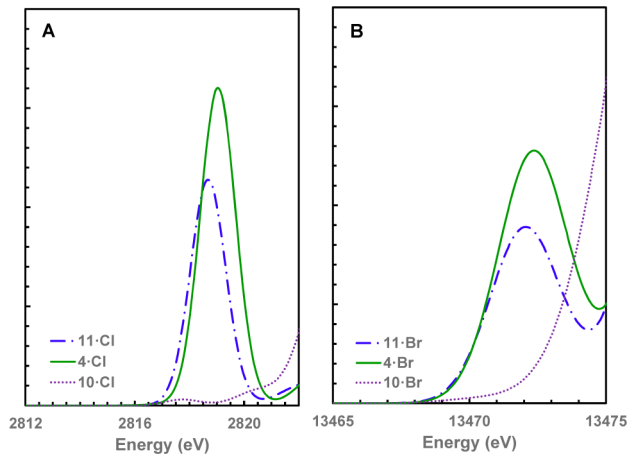

Figure 9. TDDFT simulated Cl K-edge (left) and Br K-edge (right) XAS spectra for selected XB adducts. A constant linear shift[82] was applied to the calculated energies to better match experimental K-edge energies. TDDFT details are given in section S7.

X_{1s} pre-edge transitions correlate with the degree of charge transfer from the halide to the acceptor. The trends observed in the TDDFT-calculated intensities of the transitions are in reasonable agreement with those observed in the experimental data. However, the calculated pre-edge intensities (and calculated XB charge donation) are in good agreement with those obtained from the Cl K-edge XAS data. Trends observed in pre-edge transition energies are also reproduced in the DFT results. A small shift to higher energy (∼0.4 eV) on going from a single XB acceptor (**11**·Cl) to two acceptors (in **4**·Cl) is consistent with a similar shift observed in the experimental data (see Table 4). This shift correlates with decreased electron density on the chloride, which leads to stabilization of the Cl_{1s} donor orbital.

The bromide adducts show similar trends as those observed in the chlorides; the TDDFT simulations are also in reasonable agreement with the Br K-edge experimental data. The calculated degree of charge donation is very similar between the two halides, suggesting that the degree of covalent mixing is similar in both cases. Investigations are currently underway to further evaluate the specific factors that affect the covalency of these XB interactions and the resultant binding affinities in the catenanes.

CONCLUSION

In conclusion, the XB bis-iodotriazole-pyridinium motif is shown to be a potent anion-coordinating motif in competitive aqueous media, especially when incorporated into a [2]-catenane host structural framework. The acyclic XB receptor displays a marked enhancement in anion recognition over the HB analogue and the first instance of acetate selectivity. Moreover, the XB [2]catenane notably exhibits further augmentation of anion recognition ability over its HB analogue, selectively binding halides very strongly in competitive aqueous media with no binding of oxoanions which is the reverse acetate selectivity trend of the acyclic XB receptor. This suggests the XB catenane's unique interlocked host binding cavity is of complementary size and shape for halides, whereas the oxoanions are too large and are of the wrong geometry for encapsulation.

Single crystal X-ray structural analysis provided solid-state evidence for the association of anions with the [2]catenane host framework where halide anions are able to penetrate the cavity of the [2]catenane. By contrast oxoanions ($H_2PO_4^-$ and SO_4^{2-}) are found outside the three-dimensional binding pocket in support of the solution-state anion recognition binding observations.

Cl and Br K-edge XAS revealed the presence of intense pre-edge features characteristic of charge transfer between the halide donor and the XB acceptor. Quantitative fitting of these pre-edge features provided a direct measure of the degree of covalency in the halogen bonding interaction, which is comparable to that observed in transition metal complexes. Furthermore, we confirm that perpendicular XB interactions are independent and additive, but that the degree of XB covalency can be mitigated through the presence of HB donors. These conclusions are well supported and substantiated by TDDFT simulations of the XAS data, which indicate that the degree of covalency is essentially the same for both Cl^- and Br^- donors.

Most importantly, these results offer the first evidence of this kind for covalency[83] in halogen bonds of anion receptors with halide anions. Furthermore, the presence of both XB and HB donors in the [2]catenane host framework provides interesting insight into the interplay between these two competing interactions in a single anion receptor system.

ASSOCIATED CONTENT

Supporting Information

Experimental procedures and spectroscopic data for all new compounds, titration protocol and data, full crystallographic data, XAS data and fitting details, and DFT and TDDFT computational details are available. This material is available free of charge via the Internet at http://pubs.acs.org.

dx.doi.org/10.1021/ja511648d | J. Am. Chem. Soc. 2015, 137, 499−507

AUTHOR INFORMATION

Corresponding Authors

paul.beer@chem.ox.ac.uk
pierre.kennepohl@ubc.ca

Notes

The authors declare no competing financial interest.

ACKNOWLEDGMENTS

S.W.R. thanks the Clarendon Fund and St. John's College, Oxford for funding. N.G.W. thanks the Clarendon Fund and Trinity College, Oxford for funding. A.B. thanks the Wellcome Trust and European Research Council for postdoctoral funding, ERC Advanced Grant Agreement Number 267426. The authors would like to thank Diamond Light Source for an award of beamtime on beamline I19 (MT9981). Use of the Stanford Synchrotron Radiation Lightsource, SLAC National Accelerator Laboratory, is supported by the U.S. Department of Energy, Office of Science, Office of Basic Energy Sciences under Contract No. DE-AC02-76SF00515. The SSRL Structural Molecular Biology Program is supported by the DOE Office of Biological and Environmental Research and by the National Institutes of Health, National Institute of General Medical Sciences (including P41GM103393).

REFERENCES

(1) Metrangolo, P.; Meyer, F.; Pilati, T.; Resnati, G.; Terraneo, G. *Angew. Chem., Int. Ed.* **2008**, *47*, 6114−6127.
(2) Metrangolo, P.; Neukirch, H.; Pilati, T.; Resnati, G. *Acc. Chem. Res.* **2005**, *38*, 386−395.
(3) Politzer, P.; Lane, P.; Concha, M.; Ma, Y.; Murray, J. *J. Mol. Model.* **2007**, *13*, 305−311.
(4) Erdelyi, M. *Chem. Soc. Rev.* **2012**, *41*, 3547−3557.
(5) Rissanen, K. *CrystEngComm* **2008**, *10*, 1107−1113.
(6) Brammer, L.; Espallargas, G. M.; Libri, S. *CrystEngComm* **2008**, *10*, 1712−1727.
(7) Metrangolo, P.; Pilati, T.; Terraneo, G.; Biella, S.; Resnati, G. *CrystEngComm* **2009**, *11*, 1187−1196.
(8) Gonnade, R. G.; Shashidhar, M. S.; Bhadbhade, M. M. *J. Indian Inst. Sci.* **2007**, *87*, 149−164.
(9) Fourmigué, M. *Curr. Opin. Solid State Mater. Sci.* **2009**, *13*, 36−45.
(10) Troff, R. W.; Mäkelä, T.; Topič, F.; Valkonen, A.; Raatikainen, K.; Rissanen, K. *Eur. J. Org. Chem.* **2013**, 1617−1637.
(11) Aakeröy, C. B.; Champness, N. R.; Janiak, C. *CrystEngComm* **2010**, *12*, 22.
(12) Mukherjee, A.; Tothadi, S.; Desiraju, G. R. *Acc. Chem. Res.* **2014**, *47*, 2514−2524.
(13) Metrangolo, P.; Resnati, G.; Pilati, T.; Liantonio, R.; Meyer, F. *J. Polym. Sci., Part A: Polym. Chem.* **2007**, *45*, 1−15.
(14) Meyer, F.; Dubois, P. *CrystEngComm* **2013**, *15*, 3058−3071.
(15) Priimagi, A.; Cavallo, G.; Metrangolo, P.; Resnati, G. *Acc. Chem. Res.* **2013**, *46*, 2686−2695.
(16) Castelli, R.; Schindler, S.; Walter, S. M.; Kniep, F.; Overkleeft, H. S.; Van Der Marel, G. A.; Huber, S. M.; Codée, J. D. C. *Chem.—Asian J.* **2014**, *9*, 2095−2098.
(17) Jungbauer, S. H.; Walter, S. M.; Schindler, S.; Rout, L.; Kniep, F.; Huber, S. M. *Chem. Commun. (Cambridge, U. K.)* **2014**, *50*, 6281−6284.
(18) Walter, S. M.; Sarwar, M. G.; Chudzinski, M. G.; Herdtweck, E.; Lough, A. J.; Huber, S. M.; Taylor, M. S. *CrystEngComm* **2013**, *15*, 3097−3101.
(19) Kniep, F.; Jungbauer, S. H.; Zhang, Q.; Walter, S. M.; Schindler, S.; Schnapperelle, I.; Herdtweck, E.; Huber, S. M. *Angew. Chem., Int. Ed. Engl.* **2013**, *52*, 7028−7032.
(20) Jungbauer, S. H.; Schindler, S.; Kniep, F.; Walter, S. M.; Rout, L.; Huber, S. M. *Synlett* **2013**, *24*, 2624−2628.
(21) Gilday, L. C.; Lang, T.; Caballero, A.; Costa, P. J.; Félix, V.; Beer, P. D. *Angew. Chem., Int. Ed.* **2013**, *52*, 4356−4360.
(22) Serpell, C. J.; Kilah, N. L.; Costa, P. J.; Félix, V.; Beer, P. D. *Angew. Chem., Int. Ed.* **2010**, *49*, 5322−5326.
(23) Vargas Jentzsch, A.; Hennig, A.; Mareda, J.; Matile, S. *Acc. Chem. Res.* **2013**, *46*, 2791−2800.
(24) Wilcken, R.; Zimmermann, M. O.; Lange, A.; Joerger, A. C.; Boeckler, F. M. *J. Med. Chem.* **2012**, *56*, 1363−1388.
(25) Beer, P. D.; Gale, P. A. *Angew. Chem., Int. Ed.* **2001**, *40*, 486−516.
(26) Sessler, J. L.; Gale, P. A.; Cho, W. S. *Anion Receptor Chemistry*; Royal Society of Chemistry: 2006.
(27) Evans, N. H.; Beer, P. D. *Angew. Chem., Int. Ed.* **2014**, *53*, 11716−11754.
(28) Gale, P. A.; Garcia-Garrido, S. E.; Garric, J. *Chem. Soc. Rev.* **2008**, *37*, 151−190.
(29) Gunnlaugsson, T.; Glynn, M.; Tocci, G. M.; Kruger, P. E.; Pfeffer, F. M. *Coord. Chem. Rev.* **2006**, *250*, 3094−3117.
(30) Hua, Y.; Flood, A. H. *Chem. Soc. Rev.* **2010**, *39*, 1262.
(31) Kubik, S. *Chem. Soc. Rev.* **2009**, *38*, 585−605.
(32) Llinares, J. M.; Powell, D.; Bowman-James, K. *Coord. Chem. Rev.* **2003**, *240*, 57−75.
(33) Martínez-Máñez, R.; Sancenón, F. *Coord. Chem. Rev.* **2006**, *250*, 3081−3093.
(34) O'Neil, E. J.; Smith, B. D. *Coord. Chem. Rev.* **2006**, *250*, 3068−3080.
(35) Perez, J.; Riera, L. *Chem. Soc. Rev.* **2008**, *37*, 2658−2667.
(36) Rice, C. R. *Coord. Chem. Rev.* **2006**, *250*, 3190−3199.
(37) Steed, J. W. *Chem. Soc. Rev.* **2009**, *38*, 506−519.
(38) Kavallieratos, K.; Bertao, C. M.; Crabtree, R. H. *J. Org. Chem.* **1999**, *64*, 1675−1683.
(39) Cai, J.; Sessler, J. L. *Chem. Soc. Rev.* **2014**, *43*, 6198−6213.
(40) Dutta, R.; Ghosh, P. *Chem. Commun. (Cambridge, U. K.)* **2014**, *50*, 10538−10554.
(41) Kim, S. K.; Sessler, J. L. *Acc. Chem. Res.* **2014**, *47*, 2525−2536.
(42) Langton, M. J.; Beer, P. D. *Acc. Chem. Res.* **2014**, *47*, 1935−1949.
(43) White, N. G.; Colaço, A. R.; Marques, I.; Félix, V.; Beer, P. D. *Org. Biomol. Chem.* **2014**, *12*, 4924−4931.
(44) Langton, M. J.; Beer, P. D. *Chem.—Eur. J.* **2012**, *18*, 14406−14412.
(45) Langton, M. J.; Beer, P. D. *Chem. Commun. (Cambridge, U. K.)* **2014**, *50*, 8124−8127.
(46) Langton, M. J.; Duckworth, L. C.; Beer, P. D. *Chem. Commun. (Cambridge, U. K.)* **2013**, *49*, 8608−8610.
(47) Hua, Y.; Flood, A. H. *J. Am. Chem. Soc.* **2010**, *132*, 12838−12840.
(48) Hua, Y.; Ramabhadran, R. O.; Karty, J. A.; Raghavachari, K.; Flood, A. H. *Chem. Commun. (Cambridge, U. K.)* **2011**, *47*, 5979−5981.
(49) Hua, Y.; Ramabhadran, R. O.; Uduehi, E. O.; Karty, J. A.; Raghavachari, K.; Flood, A. H. *Chem.—Eur. J.* **2011**, *17*, 312−321.
(50) Arunachalam, M.; Ravikumar, I.; Ghosh, P. *J. Org. Chem.* **2008**, *73*, 9144−9147.
(51) Ballester, P. *Chem. Soc. Rev.* **2010**, *39*, 3810−3830.
(52) Caballero, A.; White, N. G.; Beer, P. D. *Angew. Chem., Int. Ed.* **2011**, *50*, 1845−1848.
(53) Kilah, N. L.; Wise, M. D.; Serpell, C. J.; Thompson, A. L.; White, N. G.; Christensen, K. E.; Beer, P. D. *J. Am. Chem. Soc.* **2010**, *132*, 11893−11895.
(54) Mele, A.; Metrangolo, P.; Neukirch, H.; Pilati, T.; Resnati, G. *J. Am. Chem. Soc.* **2005**, *127*, 14972−14973.
(55) Sarwar, M. G.; Dragisic, B.; Sagoo, S.; Taylor, M. S. *Angew. Chem., Int. Ed.* **2010**, *49*, 1674−1677.
(56) Beale, T. M.; Chudzinski, M. G.; Sarwar, M. G.; Taylor, M. S. *Chem. Soc. Rev.* **2013**, *42*, 1667−1680.
(57) Zapata, F.; Caballero, A.; Molina, P.; Alkorta, I.; Elguero, J. *J. Org. Chem.* **2014**, *79*, 6959−6969.
(58) Gilday, L. C.; Beer, P. D. *Chem.—Eur. J.* **2014**, *20*, 8379−8385.

(59) Mullaney, B. R.; Thompson, A. L.; Beer, P. D. *Angew. Chem., Int. Ed.* **2014**, *53*, 11458−11562.
(60) Cametti, M.; Raatikainen, K.; Metrangolo, P.; Pilati, T.; Terraneo, G.; Resnati, G. *Org. Biomol. Chem.* **2012**, *10*, 1329−1333.
(61) Mercurio, J. M.; Knighton, R. C.; Cookson, J.; Beer, P. D. *Chem.—Eur. J.* **2014**, *20*, 11740−11749.
(62) Mullaney, B. R.; Partridge, B. E.; Beer, P. D. *Chem.—Eur. J.* **2014**, DOI: 10.1002/chem.201405578.
(63) Goto, H.; Heemstra, J. M.; Hill, D. J.; Moore, J. S. *Org. Lett.* **2004**, *6*, 889−892.
(64) White, N. G.; Beer, P. D. *Chem. Commun. (Cambridge, U. K.)* **2012**, *48*, 8499−8501.
(65) Alvarez, S. G.; Alvarez, M. T. *Synthesis* **1997**, *1997*, 413−414.
(66) White, N. G.; Serpell, C. J.; Beer, P. D. *Cryst. Growth Des.* **2014**, *14*, 3472−3479.
(67) Brotherton, W. S.; Clark, R. J.; Zhu, L. *J. Org. Chem.* **2012**, *77*, 6443−6455.
(68) Hynes, M. J. *J. Chem. Soc., Dalton Trans.* **1993**, 311.
(69) Single crystal X-ray diffraction data for the catenane structures were collected using synchrotron radiation at Diamond Lightsource (Nowell, H.; Barnett, S. A.; Christensen, K. E.; Teat, S. J.; Allan, D. R. *J. Synchrotron Rad.* **2012**, *19*, 435). Raw frame data (including data reduction, inter-frame scaling, unit cell refinement, and absorption corrections) were processed using CrysAlis Pro (Agilent Technologies, 2010). Structures were solved using SUPERFLIP (Palatinus, L.; Chapuis, G. *J. Appl. Crystallogr.* **2007**, *40*, 786) and refinedusing CRYSTALS (Betteridge, P. W.; Carruthers, J. R.; Cooper, R. I.; Prout, K.; Watkin, D. J. *J. Appl. Crystallogr.* **2003**, *36*, 1487 . Cooper, R. I.; Thompson, A. L.; Watkin, D. J. *J. Appl. Crystallogr.* **2010**, *43*, 1100). For further details for all crystallography, see the Supporting Information.
(70) Bondi, A. *J. Phys. Chem.* **1964**, *68*, 441−451.
(71) Wisner, J. A.; Beer, P. D.; Drew, M. G. B. *Angew. Chem., Int. Ed.* **2001**, *40*, 3606−3609.
(72) The internal pyridinium proton *c* could not be followed as shifts caused it to overlap with other resonances as anions were added.
(73) Attempts were made to quantify anion association constants in aqueous solvent mixtures containing greater percentages of D_2O; however, solubility did not allow for this.
(74) Glaser, T.; Hedman, B.; Hodgson, K. O.; Solomon, E. I. *Acc. Chem. Res.* **2000**, *33*, 859−868.
(75) Shadle, S. E.; Hedman, B.; Hodgson, K. O.; Solomon, E. I. *Inorg. Chem.* **1994**, *33*, 4235−4244.
(76) Solomon, E. I.; Hedman, B.; Hodgson, K. O.; Dey, A.; Szilagyi, R. K. *Coord. Chem. Rev.* **2005**, *249*, 97−129.
(77) Delgado-Jaime, M. U.; Conrad, J. C.; Fogg, D. E.; Kennepohl, P. *Inorg. Chim. Acta* **2006**, *359*, 3042−3047.
(78) Delgado-Jaime, M. U.; Kennepohl, P. *J. Synchrotron Rad.* **2010**, *17*, 119−128.
(79) Delgado-Jaime, M. U.; Mewis, C. P.; Kennepohl, P. *J. Synchrotron Rad.* **2010**, *17*, 132−137.
(80) Rosokha, S. V.; Stern, C. L.; Ritzert, J. T. *Chem.—Eur. J.* **2013**, *19*, 8774−8788.
(81) Neese, F. *WIREs Comput. Mol. Sci.* **2012**, *2*, 73−78.
(82) DeBeer George, S.; Petrenko, T.; Neese, F. *Inorg. Chim. Acta* **2008**, *361*, 965−972.
(83) Hunter and co-workers have recently demonstrated that the halogen bond formed between tetramethylthiourea and molecular iodine is insensitive to the nature of the organic solvent, where association constants determined in alkanes and alcohols are similar in magnitude, suggesting charge transfer interactions are making a significant contribution to the halogen bond. See: Robertson, C. C.; Perutz, R. N.; Brammer, L.; Hunter, C. A. *Chem. Sci.* **2014**, *5*, 4179−4183.